Journal of Alloys and Compounds 506 (2010) 356–363

Contents lists available at ScienceDirect

Journal of Alloys and Compounds

journal homepage: www.elsevier.com/locate/jallcom

Laser remelting of plasma-sprayed conventional and nanostructured Al_2O_3–13 wt.%TiO_2 coatings on titanium alloy

Chonggui Li[a,b,*], You Wang[a,*], Lixin Guo[a], Junqi He[a], Zhaoyi Pan[a], Liang Wang[a]

[a] Laboratory of Nano Surface Engineering, Department of Materials Science, Harbin Institute of Technology, Harbin 150001, PR China
[b] School of Materials Engineering, Shanghai University of Engineering Science, Shanghai 201620, PR China

ARTICLE INFO

Article history:
Received 11 May 2010
Received in revised form 28 June 2010
Accepted 30 June 2010
Available online 13 July 2010

Keywords:
Plasma spraying
Laser remelting
Coating materials
Microstructure evolution
Mechanical properties

ABSTRACT

Plasma-sprayed microstructured and nanostructured Al_2O_3–13 wt.%TiO_2 coatings were successfully deposited on Ti–6Al–4V titanium alloy substrates with commercial Metco 130 powder and as-prepared nanostructured feedstock, respectively. The as-sprayed coatings were remelted by a CO_2 laser to further enhance their compactness and bonding strength. The effects of laser remelting on the microstructure, phase constituents and mechanical properties of the ceramic coatings were investigated by scanning electron microscope, X-ray diffractometer and Vickers microhardness tester. The results indicate that the laser-remelted coatings exhibit more compact and homogenous structure as well as strong metallurgical bonding to the substrates. The dominating metastable γ-Al_2O_3 phase in the as-sprayed coatings transforms to stable α-Al_2O_3 during laser remelting. The microhardness value of the as-sprayed Metco 130 and nanostructured Al_2O_3–13 wt.%TiO_2 coatings is in the range of 700–1000 $HV_{0.3}$, while the microhardness values of the corresponding remelted coatings are enhanced to 1000–1350 $HV_{0.3}$ and 1100–1800 $HV_{0.3}$, respectively. With the decrease of laser scanning velocity, the microhardness is increased.

1. Introduction

Titanium is the ninth most abundant element and the fourth most abundant structural metal in the Earth's crust, and has also been detected in meteorites, the Moon, the Sun and other stars [1,2]. Owing to its high specific strength, low elastic modulus, good resistance to corrosion as well as high melting point, titanium and its alloys have found wide applications in a diverse range of fields as key structural components, including aerospace, chemical and marine industries [3–5]. However, titanium and its alloys have poor wear and abrasion resistance because of their low hardness, which definitely hampers their potential wider applications [6,7]. Preparation of a protective coating offering superior surface performances such as high hardness on the surfaces of titanium and its alloys is a promising solution to improve their surface properties while keeping the advantageous bulk properties unaffected.

Many techniques including thermal oxidation [8], physical vapor deposition [9], plasma spraying [10] and microarc oxidation [11] have been proposed to fabricate a hard and wear resistant coating on the titanium components. Among these, plasma spraying is most widely used because of its simplicity and versatility [12,13]. Plasma-sprayed Al_2O_3 and Al_2O_3–TiO_2 ceramic coatings have been developed for a wide variety of applications that require resistance to wear, erosion and corrosion due to their thermal, chemical and mechanical stability [14]. Unfortunately, limited bonding strength at the coating–substrate interface and high porosity are two major shortcomings of plasma spraying [15,16]. However, such defects are eliminable by post-laser treatment. Many investigations of post-treatment by laser have been performed on the plasma-sprayed coatings, which may contribute to the enhancement of the coating strength and chemical homogeneity, elimination of high porosity, as well as the development of a metallurgical bonding at the coating–substrate interface providing strengthened coating adhesion [17–19].

Over the past decades, nanostructured materials have been the focus of scientific research due to their superior properties associated with a nanostructure [20,21]. Compared with their conventional counterparts, plasma-sprayed nanostructured Al_2O_3–13 wt.%TiO_2 coatings derived from agglomerated feedstocks have been reported to exhibit novel and attractive properties such as high bonding strength, superior toughness, abrasive wear and corrosion resistance [22–24]. To date, extensive investigations have been done on laser surface remelting of plasma-sprayed conventional Al_2O_3–TiO_2 ceramic coatings [25–27]. Nevertheless, few investigations on laser remelting of plasma-sprayed

* Corresponding authors at: Laboratory of Nano Surface Engineering, Department of Materials Science, Harbin Institute of Technology, Harbin 150001, PR China. Tel.: +86 451 86402752; fax: +86 451 86413922.
E-mail addresses: chongguili@gmail.com (C.G. Li), wangyou@hit.edu.cn (Y. Wang).

0925-8388/$ – see front matter © 2010 Elsevier B.V. All rights reserved.
doi:10.1016/j.jallcom.2010.06.207

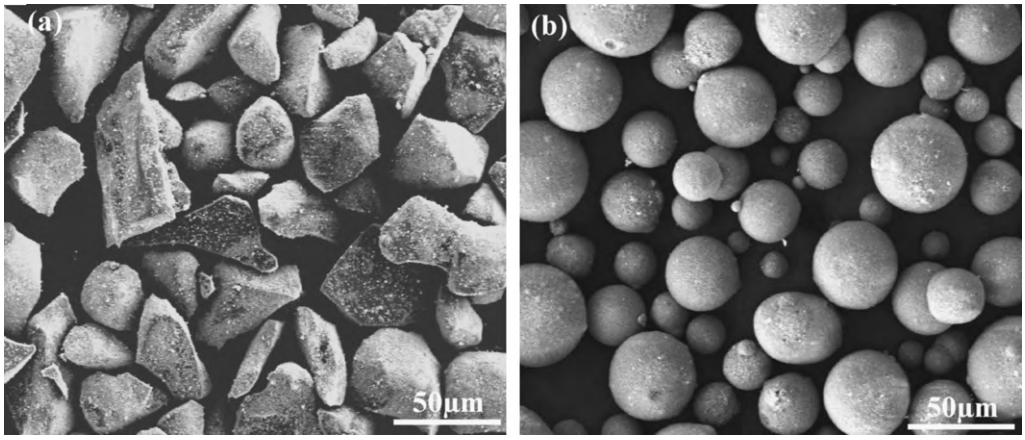

Fig. 1. Scanning electron micrographs of the Al_2O_3–13 wt.%TiO_2 feedstock used for plasma spraying: (a) as-received conventional Metco 130 powders and (b) as-prepared nanostructured powders.

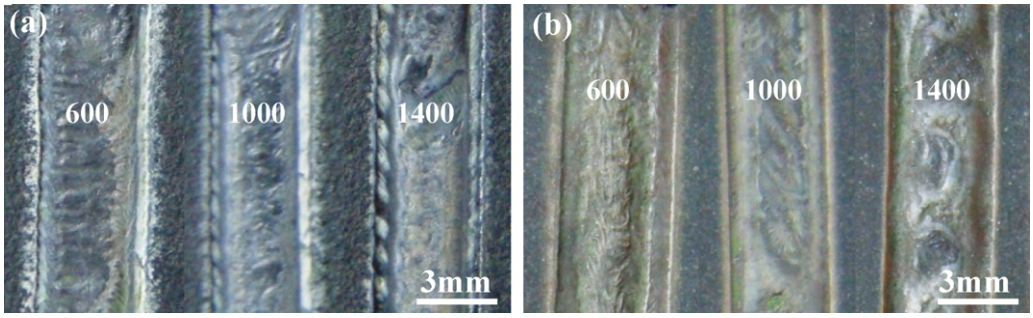

Fig. 2. Digital macro-photographs of LRmC: (a) C–LRmC and (b) N–LRmC (600, 1000 and 1400 correspond to Experimental No. 1, No. 3 and No. 5, respectively).

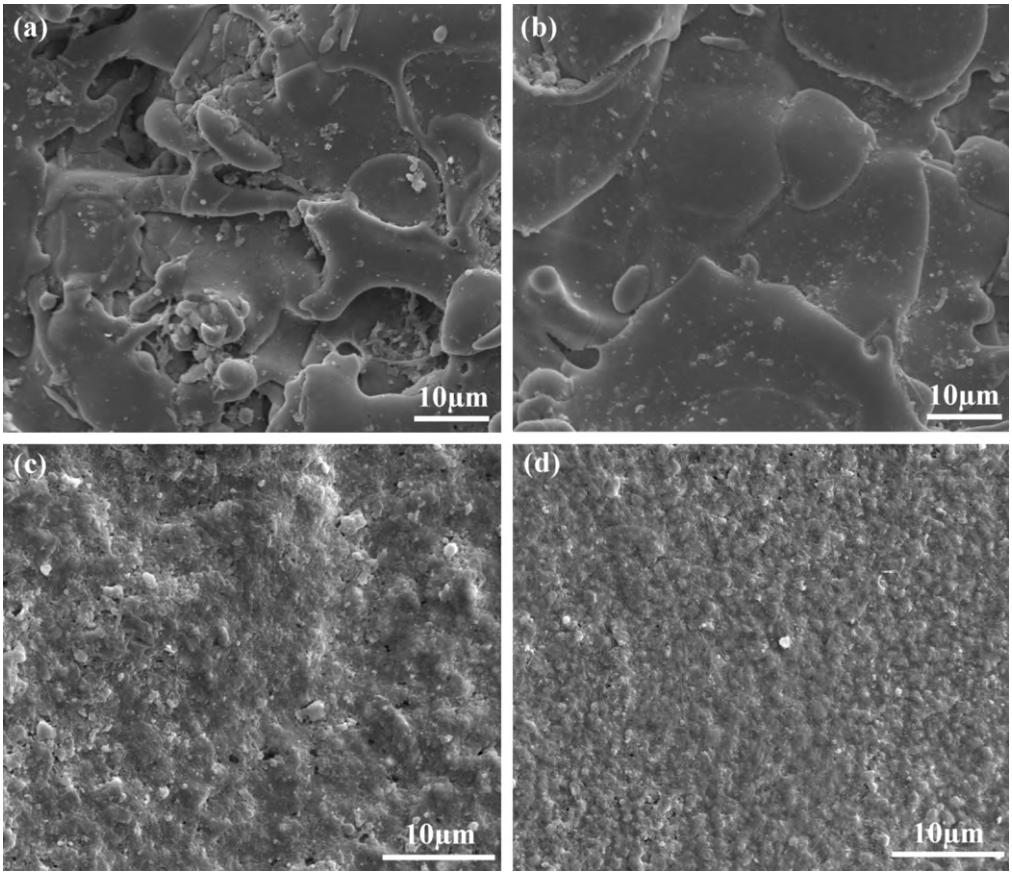

Fig. 3. Surface morphologies of (a) as-sprayed conventional Metco 130 coatings, (b) as-sprayed nanostructured Al_2O_3–13 wt.%TiO_2 coatings, (c) C–LRmC, and (d) N–LRmC.

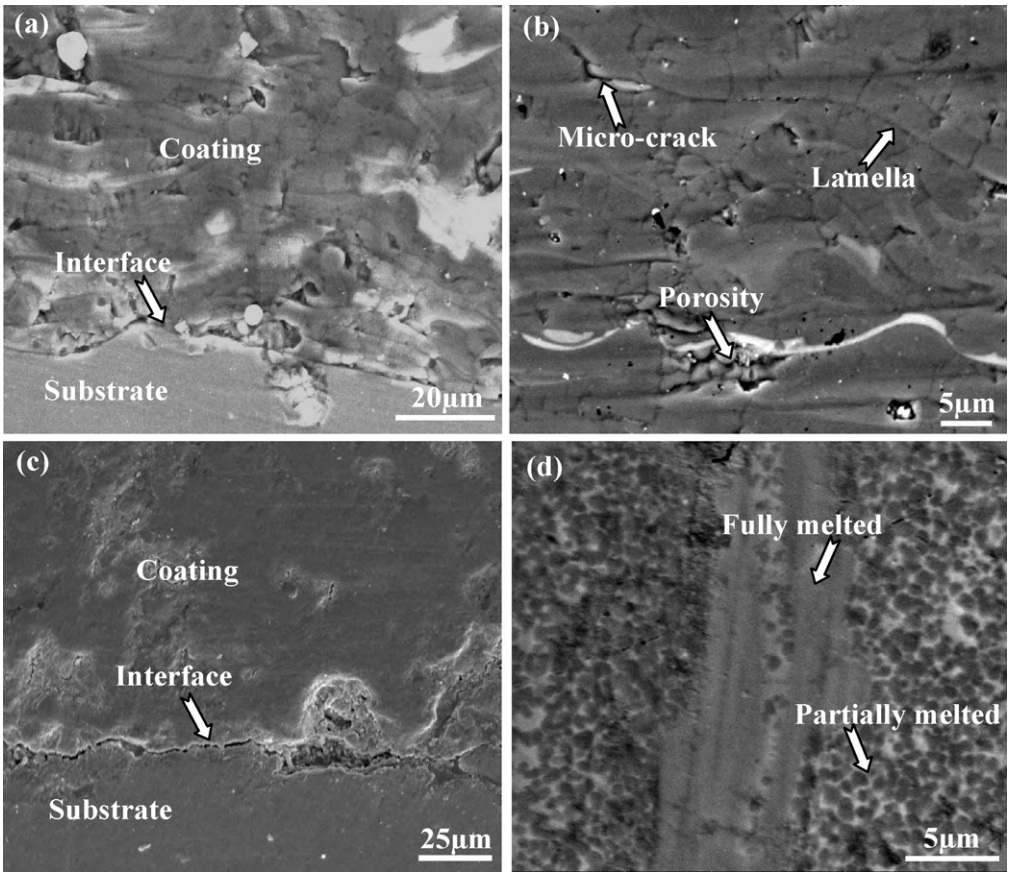

Fig. 4. Cross-sectional scanning electron micrographs of as-sprayed Al_2O_3–13 wt.%TiO_2 coatings: (a) and (b) micrographs of conventional Metco 130 coatings showing a typical mechanical bonding at the substrate-coating interface and a representative lamella stacking structure with micro-cracks and pores, respectively; (c) and (d) micrographs of nanostructured coatings showing the bonding state and a typical bimodal structure consisting of the fully melted region and partially melted region, corresponding to fused structure and three-dimensional net structure, respectively.

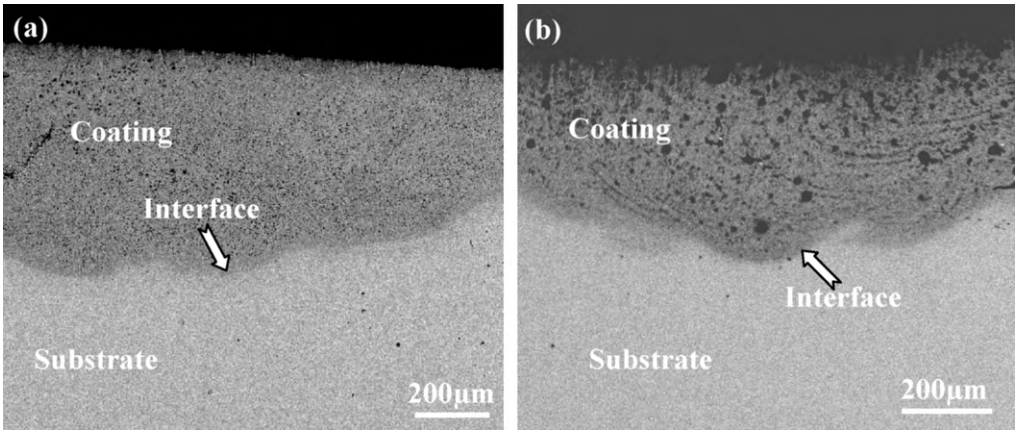

Fig. 5. Backscattered electron micrographs of LRmC showing an excellent metallurgical bonding without interface porosity between the coating and substrate: (a) C–LRmC and (b) N–LRmC.

Table 1
Parameters of laser remelting.

Experimental No.	Laser power (W)	Scanning velocity (mm/min)	Beam size (mm)	Laser output energy density (J/mm^2)	Laser power per area unit (W/mm^2)
1	1000	600	3.5	28.6	103.9
2	1000	800	3.5	21.4	103.9
3	1000	1000	3.5	17.1	103.9
4	1000	1200	3.5	14.3	103.9
5	1000	1400	3.5	12.2	103.9

The laser output energy density (laser energy per area unit) $J = P/VD$, where P is the laser power [W], D is the beam size [mm], V is the scanning velocity [mm/s]. The laser power per area unit $E = 4P/\pi D^2$, where P is the laser power [W], D is the beam size [mm].

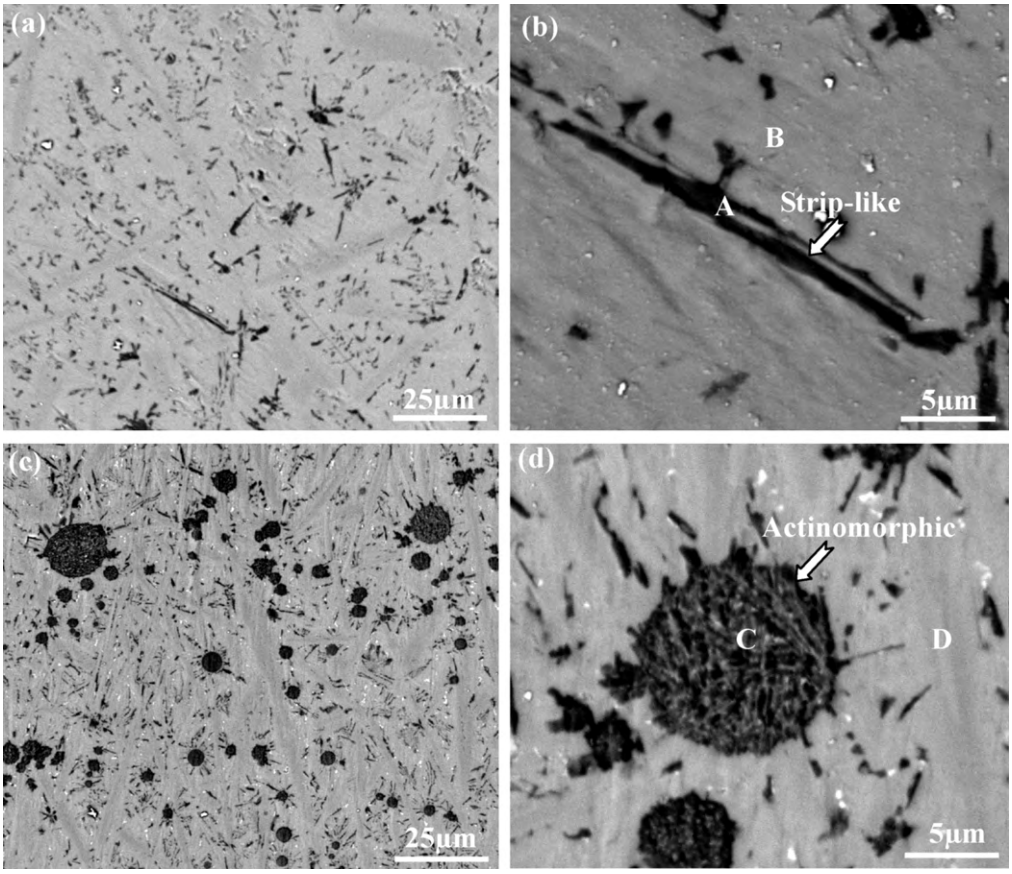

Fig. 6. Backscattered electron micrographs of (a) and (b) C–LRmC showing the long strip-like microstructure, (c) and (d) N–LRmC showing the actinomorphic microstructure, (b) and (d) are high magnification micrographs of (a) and (c), respectively.

nanostructured Al_2O_3–TiO_2 coatings have been performed [28,29]. Furthermore, to our knowledge, a comparative study on laser surface remelting of plasma-sprayed conventional and nanostructured Al_2O_3–13 wt.%TiO_2 coatings has never been reported yet. The purpose of this work is to investigate the effects of laser remelting on the microstructure, phase constituents and mechanical properties of the as-sprayed conventional and nanostructured Al_2O_3–13 wt.%TiO_2 coatings, focusing on the microstructure evolution at different stages of the preparation processes, i.e., starting feedstock powders – plasma-sprayed coatings – remelted coatings.

2. Experimental procedures

2.1. Substrate material

The substrate material used in the present study was a Ti–6Al–4V titanium alloy. The chemical composition (wt.%) of the as-received substrate material is listed as follows: 6.00 Al, 4.30V, 0.30 Fe, 0.10 Si, 0.10 C, 0.15 O, and the balance is Ti. Samples were cut into slabs with the size of 57 mm × 25 mm × 6 mm by electrical discharge machining.

2.2. Feedstock powders

In the present work, two types of powders were used as feedstocks for the deposition of the conventional and nanostructured coatings. One was a commercially available micrometer-sized Metco 130 powder (Sulzer Metco Co., Ltd., USA). The chemical composition of the Metco powder particles was 87 wt.% Al_2O_3 and 13 wt.% TiO_2. Fig. 1a shows the scanning electron micrograph of the Metco 130 powders. As a fused and crushed powder, it exhibits irregular and angular features. The other was reconstituted agglomerates derived from nanoparticles. The raw material powders consisted of Al_2O_3 (δ and γ phases, 99.9% purity, Degussa Co., Ltd., Germany) with particle size of 20–45 nm, TiO_2 (anatase, 99.9% purity, Nanjing High Technology Nano Materials Co., Ltd., China) with particle size of 20–50 nm, ZrO_2 (tetragonal phase, 99.9% purity, Cug-Nano Materials Manufacturing Co., Ltd., China) with particle size of 20–50 nm and CeO_2 (cubic phase, 99.9% purity, Rare Chem. Co., Ltd., China) with particle size of 20–40 nm. Al_2O_3 and TiO_2 were the main compositions with a mass ratio of 87:13. ZrO_2 and CeO_2 were used as additives and their weight content was about 5%, respectively. All the nanoparticles were mixed by wet ball milling for 24 h. A certain amount of polyvinyl alcohol (PVA) emulsion was added into the slurry as a binder. The as-prepared nanostructured Al_2O_3–13 wt.%TiO_2 feedstock powders were obtained by subsequent spray drying, sintering and plasma treatment. The sintering was conducted in a furnace with a temperature of 1200 °C and a sintering time of 3 h. During the plasma treatment, the powders passed a plasma flame generated by a Metco 9MB gun (Sulzer Metco, USA) in a very short time. The scanning electron micrograph of the nanostructured feedstock is shown in Fig. 1b. It presents a regular spherical morphology with smooth surface. The size of the feedstock powders is in the range of 20–50 μm.

2.3. Plasma spraying and post-laser remelting

Atmospheric plasma spraying was used to deposit the nanostructured coatings on ultrasonic-cleaned and freshly grit-blasted Ti–6Al–4V titanium alloy substrates. The plasma spraying was performed by a Metco 9M plasma spray control system with a Metco 9MB gun (Sulzer Metco, USA). A mixture of Ar and H_2 was used as the plasma gas and Ar was used as the powder carrier gas. The parameters of plasma spraying were as follows: (a) current was 600 A, (b) voltage was 65 V, (c) primary Ar gas pressure was about 690 kPa, (d) secondary H_2 gas pressure was about 380 kPa, (e) Ar gas flow rate was 120 SCFH (standard cubic feet per hour), (f) powder feed rate was 1000–1500 g/h, and (g) spray distance was about 100 mm. The thickness of the as-sprayed coatings is in the range of 200–300 μm.

The as-sprayed coatings were subsequently remelted by a continuous wave CO_2 laser (DL-HL-T5000, China) operated at a wavelength of 10.6 μm with a maximum output power of 5 kW. The laser beam was defocused to a spot of 3.5 mm in diameter at the surface of the coatings. The laser output power used in this study was 1000 W. The parameter details of laser remelting are listed in Table 1.

For short, the laser-remelted Al_2O_3–13 wt.%TiO_2 coatings are referred to as LRmC. The LRmC derived from as-sprayed conventional Metco 130 coatings and nanostructured Al_2O_3–13 wt.%TiO_2 coatings are referred to as C–LRmC and N–LRmC, respectively.

Fig. 2 shows the digital macro-photographs of the LRmC taken by a digital camera. It presents flat coating surfaces. For both C–LRmC and N–LRmC, with the increase

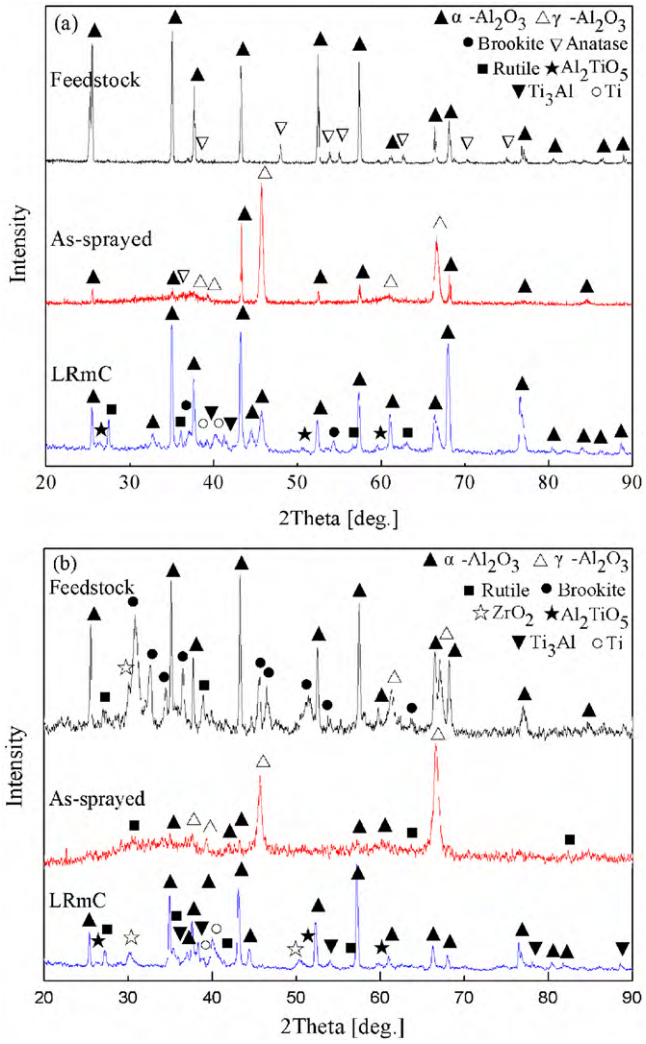

Fig. 7. XRD patterns of (a) Metco 130 feedstock powder and its coatings before and after laser remelting and (b) nanostructured Al_2O_3–13 wt.%TiO_2 feedstock powder and its coatings before and after laser remelting.

of laser velocities from 600 to 1400 mm/min, the width of melting tracks is decreased while the surface roughness is increased. Under the higher scanning velocity of 1400 mm/min, the coatings are not sufficiently remelted and air pores are observed for both kinds of samples.

2.4. Characterization

The microstructure and phase constituents of the feedstock powders and the coatings before and after laser remelting were examined by a scanning electron microscope (SEM, Quanta 200, FEI, USA) equipped with X-ray energy-dispersive spectroscopy (EDS) and an X-ray diffractometer (XRD, D/max-γB, Japan, with Cu Kα radiation (λ = 0.15418 nm)). Microhardness of the cross-section of as-sprayed coatings and laser-remelted coatings (LRmC) was measured by a Vickers microhardness tester (HV-1000) under a load of 300 g with a dwell time of 15 s.

3. Results and discussion

3.1. Microstructure

The microstructure of the Al_2O_3–13 wt.%TiO_2 ceramic coatings before and after laser remelting was investigated by scanning electron microscopy. Fig. 3 shows the surface morphologies of the as-sprayed coatings and LRmC. During plasma spraying, the feedstock powders were thermally melted into liquid droplets and sprayed to the grit-blasted substrates at a high speed. The coatings were formed by a continuous build-up of liquid droplets layer by layer. The SEM observations prove that the as-sprayed coatings exhibit the typical features of porosity and irregular structure of lamellar splats. It is noted that more voids and pores are found at the surface of the Metco 130 coatings, compared with the as-sprayed nanostructured coatings (Fig. 3a and b). With the purpose to improve the coating quality, high-energy laser beam was applied to remelt the as-sprayed coatings. After laser remelting, the surface layers of the LRmC are considerably compacted, with the enhancement of homogeneity and the elimination of voids, pores and stacking features (Fig. 3c and d). In addition, compared with the C–LRmC, the N–LRmC possess more compact and smoother surface microstructure. The additives (ZrO_2 and CeO_2) may contribute to the improvement of compactness and microstructure optimization of the ceramic coatings.

Fig. 4 presents the cross-sectional scanning electron micrographs of the as-sprayed coatings. As indicated by the SEM observations, the as-sprayed ceramic coatings possess mechanical bonding to the titanium substrates (Fig. 4a and c). The mechanical bonding refers to the adherence of sprayed droplets to a roughened surface by the mechanism of mechanical interlocking of particles at high velocity. More detailed micrograph of the Metco 130 coatings presents evident lamella stacking structure. In addition, the layered structure is accompanied by some micro-cracks and pores (Fig. 4b), which is not so apparent in the as-sprayed nanostructured coatings. Further, detailed SEM micrograph of the as-sprayed nanostructured coatings (Fig. 4d) shows that these coatings exhibit a unique bimodal microstructure, which has been extensively discussed [30,31]. The bimodal distribution of microstructure consists of two distinct regions, i.e., a fully melted region and a partially melted region. The fully melted region consists of lamellar splats derived from fully melted feedstock, while the partially melted region consists of particulates of three-dimensional net structure derived from partially melted feedstock.

After post-remelting by high-energy laser beam, distinct microstructure features on cross-sectional view of the LRmC are observed. Fig. 5 shows backscattered electron micrographs of C–LRmC and N–LRmC. It can be seen that the LRmC possess a more compact and homogenous microstructure. The pre-existing pores and micro-cracks are remarkably eliminated. These are highly desirable for providing a hardened protective coating for the substrates. Further, the molten pool of the N–LRmC exhibits a distinct streamlined microstructure (Fig. 5b). It indicates the specific flow characteristics in the molten pool containing the nanostructured coating materials during laser remelting. In particular, it is evident that a metallurgical bonding without interface porosity is formed at the coating–substrate interface both for C–LRmC and N–LRmC. The metallurgical bonding refers to the adherence formed by the diffusion and solidification of the coating materials and the titanium alloy substrate. As stated above, the mechanical bonding is formed by mechanical interlocking, the strength of which has been reported to be around 15–30 MPa [30,32]. It may provide sufficient static strength at normal service conditions without repetitive stress. However, exposed to hot or wet environments requiring high reliability and durability, the coatings would be susceptible to peeling, spalling or other deterioration. With the increasing demand of competent components with high-strength serving at ever more severe application conditions such as heavy loads, high speeds and wet or hot environments, coupled with the limitations of development of high-strength bulk materials and their manufacturing techniques, the preparation of surface coatings with high performance and desired bonding strength becomes of great significance.

Fig. 6 presents the backscattered electron micrographs of C–LRmC and N–LRmC showing their distinct microstructure features. For the C–LRmC, randomly distributed strip-like microstructure is observed (Fig. 6a and b). The long strip-like microstructure

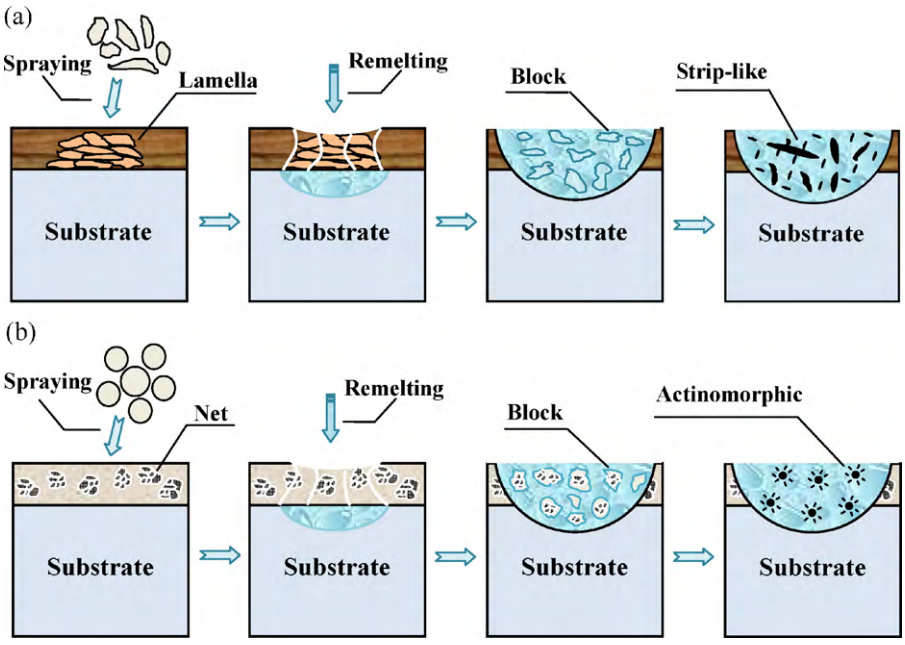

Fig. 8. Schematic illustration of a microstructure evolution model indicating the microstructure evolution at three stages of processing, i.e., starting feedstock powders – as-sprayed coatings – remelted coatings: (a) the microstructure features of Metco 130 feedstock powder and its coatings before and after laser remelting and (b) the microstructure features of nanostructured Al_2O_3–13 wt.%TiO_2 feedstock powder and its coatings before and after laser remelting.

resembles the shape of the angular Metco 130 feedstock and the lamella structure of its as-sprayed coatings. For the N–LRmC, a representative actinomorphic microstructure is observed instead (Fig. 6c and d). In this case, the actinomorphic microstructure bears an analogy to the shape of the round nanostructured Al_2O_3–13 wt.%TiO_2 feedstock powders and the features of the fine grains found within the actinomorphic microstructure are also similar to those of the net structure of its as-sprayed coatings. This interesting microstructure evolution will be described and discussed in details in a later section.

In summary, distinct features in the microstructures of the ceramic coatings before and after laser remelting have been confirmed. The lamellar defects and the pre-existing pores and cracks of the as-sprayed coatings are eliminated, and the LRmC is considerably compacted and homogenized. This is attributed to the structure refinement during the remelting process. Furthermore, the mechanical bonding of the as-sprayed coatings transforms to the metallurgical bonding by laser remelting, which is helpful to improve their bonding strength.

3.2. Phase constituents

Fig. 7 shows the X-ray diffraction patterns of the feedstock powders and their coatings before and after laser remelting. It is clear that the as-received Metco 130 feedstock powder is composed of α-Al_2O_3 and anatase-TiO_2. In its as-sprayed coating, the peaks of α-Al_2O_3, γ-Al_2O_3 and anatase-TiO_2 are indexed. After laser remelting, α-Al_2O_3, rutile-TiO_2, Brookite-TiO_2, Al_2TiO_5 and Ti_3Al are found. For the as-prepared nanostructured Al_2O_3–13 wt.%TiO_2 feedstock, the presence of α-Al_2O_3, γ-Al_2O_3, brookite-TiO_2, rutile-TiO_2 and ZrO_2 is demonstrated. In its as-sprayed coating, α-Al_2O_3, γ-Al_2O_3 and rutile-TiO_2 are found. The obtained N–LRmC is composed of α-Al_2O_3, rutile-TiO_2, ZrO_2, Al_2TiO_5 and Ti_3Al.

The XRD analysis has shown that both of the conventional and nanostructured as-sprayed coatings contain γ-Al_2O_3 as major phase and α-Al_2O_3 as minor phase, while their feedstock powders are mainly composed of α-Al_2O_3 phase. During the plasma spraying process, some α-Al_2O_3 transforms to γ-Al_2O_3. Previous studies [23,33,34] also provide similar results that the plasma-sprayed alumina coatings are dominated by γ-Al_2O_3. This indicates that the deposited spray particles have reached melting state prior to the impact on substrate [35]. The initial nucleation of metastable γ-Al_2O_3 in the as-sprayed coatings is attributed to its lower nucleating free energy. Under favorable conditions of rapid cooling and solidification process during plasma spraying (up to $5.08 \times 10^6\ K\ s^{-1}$), the γ-$Al_2O_3$ phase can be retained [36]. After laser remelting, both for the C–LRmC and N–LRmC, the metastable γ-Al_2O_3 phase transforms to thermodynamically stable α-Al_2O_3. Under the irradiation of high-energy laser beam during laser remelting, the surface temperature of the as-sprayed coating is estimated to be around 3000 K based on simulation results [36]. Consequently, the as-sprayed coating and the adjacent top substrate are melted and subsequently resolidified, favoring the transformation of γ-Al_2O_3 into α-Al_2O_3. In addition, exposed to increased temperature, TiO_2 tends to react with Al_2O_3 and Al_2TiO_5 could be formed at temperatures above 1200 °C, according to the phase diagram of Al_2O_3–TiO_2 system. The subsequent rapid cooling of the coating materials also results in the presence of Al_2TiO_5 in the LRmC at room temperature. Further, part of Ti from the substrate tends to react with Al due to their increased reactivity, and intermetallic Ti_3Al phase is formed by reaction and possible diffusion. It is also noted that the anatase-TiO_2 phase of the Metco 130 feedstock powder and its as-sprayed coating transforms to brookite-TiO2 and rutile-TiO2 after laser remelting.

3.3. Microstructure evolution

Based on the experimental observations described above, a model has been proposed to fully comprehend the microstruc-

Table 2
EDS analysis of the LRmC (at.%, the investigated spots are shown in Fig. 6b and d).

	Al	Ti	O
Point A	48.07	4.27	47.66
Point B	22.01	58.89	19.10
Point C	48.11	6.28	45.60
Point D	10.37	62.29	27.34

ture evolution at the three stages of processing, i.e., preparation of starting feedstocks – deposition of ceramic coatings by plasma spraying – post-laser treatment, as illustrated in Fig. 8. During plasma spraying, the angular microstructured Metco 130 powders are deposited on the titanium alloy substrates via stacking droplets, and the lamella splat microstructure is clearly observed in the as-deposited conventional Metco 130 coatings. By post-laser remelting, the as-sprayed coating and the adjacent top substrate are remelted and the coating materials are smashed into blocks randomly distributed in the molten pool. Finally, the strip-like microstructure is obtained in the C–LRmC. By comparison, the round nanostructured Al_2O_3–13 wt.%TiO_2 feedstock powders are deposited by plasma spraying to form a coating containing net structure. Then, after identical processing by laser, the actinomorphic microstructure is obtained in the N–LRmC, as a result of the rapid resolidification.

It is noteworthy that the shape of the angular Metco 130 feedstock powder is similar to that of the strip-like microstructure of the C–LRmC. For the nanostructured Al_2O_3–13 wt.%TiO_2 powder, its cross-sectional net structure has been confirmed by our previous investigations [28]. In its as-sprayed coating and LRmC, similar net structures are also observed in the present study. Table 2 shows the EDS analysis results of the LRmC. It can be seen that the chemical composition of the strip-like microstructure in the C–LRmC and the actinomorphic microstructure in the N–LRmC is similar to that of the feedstock powders. The higher content of Ti in the fused structure is attributed to the melting of the substrate materials into the molten pool. In addition, the ceramic coatings exhibit low thermal conductivity and thermal diffusivity. The thermal conductivity of Al_2O_3 is about 30 W m^{-1} K^{-1} and that of TiO_2 is about 9 W m^{-1} K^{-1} [25]. As a high-energy and short-duration processing, laser remelting would offer high temperature on the coating surface, while the temperature of the bottom and edge portions of the molten pool is relatively low. Thus, a specific thermal gradient might be formed along the coating thickness during laser remelting. Part of the as-sprayed coatings without sufficient heat energy would be partially melted. Finally, as indicated above, the strip-like and actinomorphic microstructures are obtained after the subsequent rapid resolidification.

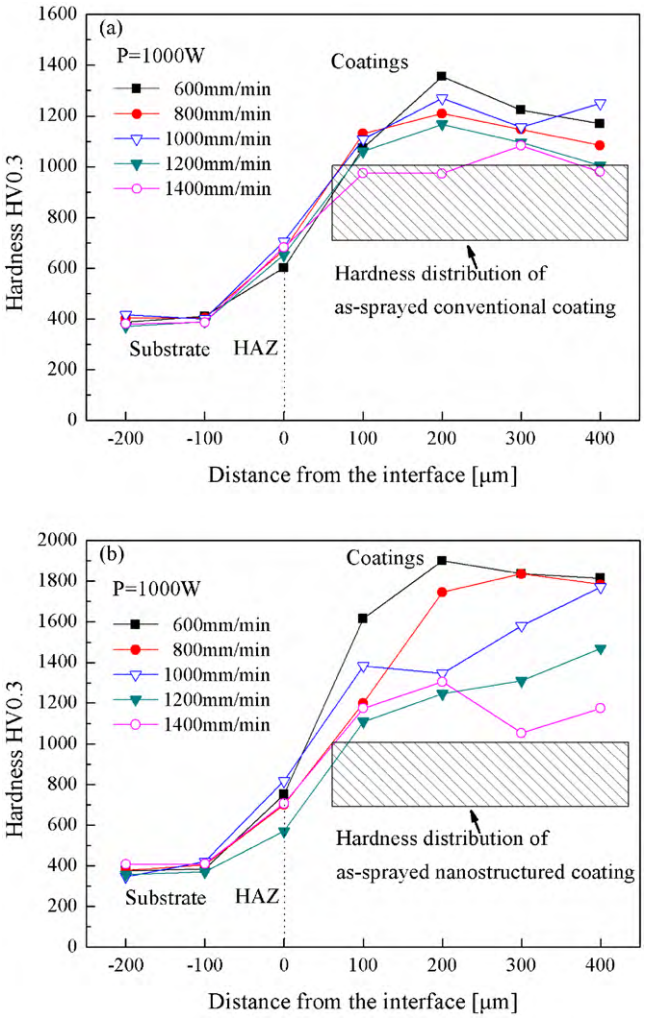

Fig. 9. Microhardness distribution of the ceramic coatings before and after laser remelting: (a) as-sprayed conventional Metco 130 coating and C–LRmC and (b) as-sprayed nanostructured Al_2O_3–13 wt.%TiO_2 coating and N–LRmC.

3.4. Hardness distribution of the coatings

Microhardness distribution of the as-sprayed coatings and LRmC as a function of the coating thickness is shown in Fig. 9. It is evident that the microhardness value of the as-received titanium alloy substrates is in the range of 350–400 $HV_{0.3}$, while the microhardness values of the as-sprayed microstructured and nanostructured coatings are in the range of 700–1000 $HV_{0.3}$. After laser remelting, the microhardness value of the C–LRmC is increased by approximately 30% to the range of 1000–1350 $HV_{0.3}$. Correspondingly, the microhardness value of the N–LRmC is increased by approximately 60% to the range of 1100–1800 $HV_{0.3}$. In addition, with the decrease of the scanning velocities of the laser beam, the microhardness of the LRmC is generally increased. This trend is more apparent for the N–LRmC.

Compared with the as-sprayed coatings, the considerably higher hardness of the LRmC is basically ascribed to their pronounced compact and homogenous microstructure as well as the formation of hard phases like α-Al_2O_3, which possesses higher hardness than γ-Al_2O_3. In addition, owing to the distinct microstructure, the N–LRmC exhibit higher hardness than the C–LRmC. The actinomorphic microstructure of the N–LRmC should be beneficial to increase the hardness of the coatings.

It is also noted that the LRmC exhibit a graded distribution of hardness, which corresponds to three regions: the substrate, the coating zone and a heat-affected zone (HAZ) next to the coating–substrate interface. The coating zone is a remelted zone, which is subjected to the remelting and resolidification process, while the HAZ is only subjected to the heating and cooling process with no melting involved [37]. The hardness of the HAZ is between that of the coating zone and the substrate.

The results indicate that laser remelting is a promising approach to prepare a hard protective ceramic coating. Ti–6Al–4V titanium alloy is one of the most widely used structural materials in the aerospace industry. The fabrication of such a hard coating with strong metallurgical bonding strength to the titanium alloy to enhance its surface properties would consequently expand its industrial applications, particularly for services at harsh environments, which are increasingly in demand.

4. Conclusions

From the results presented in this study, it is clearly indicated that laser remelting is a promising approach for the fabrication of compact Al_2O_3–13 wt.%TiO_2 coatings on Ti–6Al–4V titanium alloy. The following conclusions can be drawn: (1) the as-sprayed ceramic coatings possess mechanical bonding to the substrates. The as-sprayed Metco 130 coatings exhibit evident lamella stacking structure and the as-sprayed nanostructured coatings exhibit a

unique bimodal microstructure; (2) the remelted coatings possess a strong metallurgical bonding to the substrates without interface porosity. More compact and homogenous structure is observed in the LRmC, with the elimination of pre-existing defects and lamellae structure of the as-sprayed coatings; (3) the C–LRmC exhibit randomly distributed strip-like microstructure, while the N–LRmC possess actinomorphic microstructure; (4) the XRD analysis proves that both as-sprayed coatings are dominated by γ-Al_2O_3 phase, which transforms to thermodynamically stable α-Al_2O_3 during laser remelting; (5) the microhardness value of the as-sprayed microstructured and nanostructured coatings is in the range of 700–1000 $HV_{0.3}$, which is increased by approximately 30% to the range of 1000–1350 $HV_{0.3}$ in the C–LRmC and 60% to the range of 1100–1800 $HV_{0.3}$ in the N–LRmC. With the decrease of the laser scanning velocity, the microhardness is increased.

Acknowledgments

The authors would like to thank the Natural Science Foundation of Heilongjiang Province, China, for providing financial support. We are also grateful to Dr. B. Zhong, W. Tian, Y. Yang, F.J. Wang and S. Wang from Harbin Institute of Technology for helpful discussions and their kind assistance during our experiments.

References

[1] R. Li, A.J. Shih, Int. J. Adv. Manuf. Technol. 29 (2006) 253–261.
[2] A. Zhechevaa, W. Sha, S. Malinov, A. Long, Surf. Coat. Technol. 200 (2005) 2192–2207.
[3] N. Poondla, T.S. Srivatsan, A. Patnaik, M. Petraroli, J. Alloys Compd. 486 (2009) 162–167.
[4] Y.S. Tian, C.Z. Chen, S.T. Li, Q.H. Huo, Appl. Surf. Sci. 242 (2005) 177–184.
[5] A.N. Alhazaa, T.I. Khan, J. Alloys Compd. 494 (2010) 351–358.
[6] Q. Jin, W.B. Xue, X.J. Li, Q.Z. Zhu, X.L. Wu, J. Alloys Compd. 476 (2009) 356–359.
[7] X.Y. Liu, P.K. Chub, C.X. Ding, Mater. Sci. Eng. R 47 (2004) 49–121.
[8] A. Ashrafizadeh, F. Ashrafizadeh, J. Alloys Compd. 480 (2009) 849–852.
[9] S.R. Paital, N.B. Dahotre, J. Alloys Compd. 487 (2009) 499–503.
[10] C.G. Zhou, F. Cai, J. Kong, S.K. Gong, H.B. Xu, Surf. Coat. Technol. 187 (2004) 225–229.
[11] F. Liu, J.L. Xu, D.Z. Yu, F.P. Wang, L.C. Zhao, J. Alloys Compd. 487 (2009) 391–394.
[12] C.G. Li, Y. Wang, S. Wang, L.X. Guo, J. Alloys Compd. 503 (2010) 127–132.
[13] V Pasumarthi, Y. Chen, S.R. Bakshi, A. Agarwal, J. Alloys Compd. 484 (2009) 113–117.
[14] E.H. Jordan, M. Gell, Y.H. Sohn, D. Goberman, L. Shaw, S. Jiang, M. Wang, T.D. Xiao, Y. Wang, P. Strutt, Mater. Sci. Eng. A 301 (2001) 80–89.
[15] M. Zheng, D. Fan, X.K. Li, J.B. Zhang, Q.B. Liu, J. Alloys Compd. 489 (2010) 211–214.
[16] X.C. Zhang, B.S. Xu, F.Z. Xuan, H.D. Wang, Y.X. Wu, J. Alloys Compd. 473 (2009) 145–151.
[17] C.Z. Chen, D.G. Wang, Q.H. Bao, L. Zhang, T.Q. Lei, Appl. Surf. Sci. 250 (2005) 98–103.
[18] G.Y. Liang, T.T. Wong, J.M.K. MacAlpine, J.Y. Su, Surf. Coat. Technol. 127 (2000) 233–238.
[19] J. Mateos, J.M. Cuetos, E. Fernandez, R. Vijande, Wear 239 (2000) 274–281.
[20] Y. Yang, Y. Wang, W. Tian, Y. Zhao, J.Q. He, H.M. Bian, Z.Q. Wang, J. Alloys Compd. 481 (2009) 858–862.
[21] D. Zois, A. Lekatou, M. Vardavoulias, A. Vazdirvanidis, J. Alloys Compd. 495 (2010) 611–616.
[22] Y. Wang, S. Jiang, M.D. Wang, S.H. Wang, T.D. Xiao, P.R. Strutt, Wear 237 (2000) 176–185.
[23] L. Shaw, D. Goberman, R. Ren, M. Gell, S. Jiang, Y. Wang, T.D. Xiao, P.R. Strutt, Surf. Coat. Technol. 130 (2000) 1–8.
[24] Y. Wang, W. Tian, T. Zhang, Y. Yang, Corros. Sci. 51 (2009) 2924–2931.
[25] J. Iwaszko, Surf. Coat. Technol. 201 (2006) 3443–3451.
[26] Y.Z. Yang, Y.L. Zhu, Z.Y. Liu, Y.Z. Chuang, Mater. Sci. Eng. A 291 (2000) 168–172.
[27] L. Dubourg, R.S. Lima, C. Moreau, Surf. Coat. Technol. 201 (2007) 6278–6284.
[28] Y. Wang, C.G. Li, W. Tian, Y. Yang, Appl. Surf. Sci. 255 (2009) 8603–8610.
[29] D.S. Wang, Z.J. Tian, L.D. Shen, Z.D. Liu, Y.H. Huang, Appl. Surf. Sci. 255 (2009) 4606–4610.
[30] Y. Wang, W. Tian, Y. Yang, Surf. Coat. Technol. 201 (2007) 7746–7754.
[31] D. Goberman, Y.H. Sohn, L. Shaw, E. Jordan, M. Gell, Acta Mater. 50 (2002) 1141–1152.
[32] S. Salman, Z. Cizmecioglu, J. Mater. Sci. 33 (1998) 4207–4212.
[33] X.H. Lin, Y. Zeng, S.W. Lee, C.X. Ding, J. Eur. Ceram. Soc. 24 (2004) 627–634.
[34] R. Yılmaz, A.O. Kurt, A. Demir, Z. Tatlı, J. Eur. Ceram. Soc. 27 (2007) 1319–1323.
[35] Ş. Yılmaz, Ceram. Int. 35 (2009) 2017–2022.
[36] Y. Chen, A. Samant, K. Balani, N.B. Dahotre, A. Agarwal, Appl. Phys. A 94 (2009) 861–870.
[37] Z. Sun, I. Annergren, D. Pan, T.A. Mai, Mater. Sci. Eng. A 345 (2003) 293–300.